Substrate supply for calcite precipitation in *Emiliania huxleyi*: Assessment of different model approaches[1]
APPENDIX

Lena-Maria Holtz[2]
Alfred Wegener Institute for Polar and Marine Research, Am Handelshafen 12, 27570 Bremerhaven, Germany

Silke Thoms
Alfred Wegener Institute for Polar and Marine Research, Am Handelshafen 12, 27570 Bremerhaven, Germany

Gerald Langer
Department of Earth Sciences, Cambridge University, Downing St., Cambridge. CB2 3EQ, UK.

Dieter A. Wolf-Gladrow
Alfred Wegener Institute for Polar and Marine Research, Am Handelshafen 12, 27570 Bremerhaven, Germany

[1] Received: ; Accepted:
[2] Corresponding author, Lena-Maria.Holtz@awi.de, +49(471)4831-2093,

Appendix to Kinetic model setup

(a) Morphology of the CV

Size and morphology of the coccolith vesicle (CV) are estimated from TEM images taken from van der Wal *et al.* (1983a) and from SEM images made by Young (2009). Surface area and volume of a simplified shape (see Fig. S1) are 33 μm^2 and 3.2 μm^3, respectively, when a diameter of 3.5 μm is presumed for the coccolith, which is the coccolith size we have the calcite amount for (Young & Ziveri, 2000). The first detectable stage of the CV is the so called proto-coccolith vesicle (pCV, see Fig. 5 in van der Wal *et al.* (1983a)), for whose shape an oblate spheroid with a large radius of 0.25 μm and a small radius of 0.09 μm was assumed (A_{pCV} = 0.5 μm^2, V_{pCV} = 0.02 μm^3). Surface area and volume of the CV do not change during coccolith formation in our model in order to keep the model simple. A representative situation for calcite precipitation was chosen instead. Assuming the transporter density inside the CV membrane remains unchanged during coccolith formation, the mean value between the pCV and the full size CV should constitute a meaningful approach. The model runs are performed with the following values: 17 μm^2 for the surface area and 1.6 μm^3 for the volume of the CV. During coccolith formation, the fluid within the CV becomes actually more and more restricted to the thin layer between the growing coccolith and the CV membrane. Therefore, performing model simulations with the whole volume of the CV (1.6 μm^3) constitutes a conservative assumption.

(b) Carbonate chemistry and [Ca^{2+}]

A summary of the conditions assumed for the cytosol and as initial conditions inside the CV is given in Table S1. While all chemical characteristics of the cytosol (equilibrated carbonate system) are kept constant throughout the model runs, the corresponding values of the CV vary with time in response to the individual transported substrates and reactions of the carbonate system. The cytosolic [Ca^{2+}] is set to 100 nmol·L^{-1}, the value measured by Brownlee *et al.* (1995). The initial [Ca^{2+}] within the CV is assumed to be 0.5 mmol·L^{-1}, a value typical for the ER (Gussone *et al.*, 2006). The cytosolic DIC as well as the initial DIC inside the CV equal the seawater value in our model, i.e. 2 mmol $\cdot$ L^{-1}. Sekino & Shiraiwa (1994) measured the bulk DIC of *E. huxleyi* to be 13 mmol·L^{-1}. It is, however, very likely that DIC is not distributed evenly inside the cell. A strong accumulation of DIC inside the cytosol would probably lead to a strong diffusive CO_2 lost, further amplified by the low cytosolic pH value compared to the one of seawater. A more effective location to accumulate DIC are the organelles, in which C_i is assimilated, i.e. the chloroplast or the CV. However, since an accumulation of DIC inside the cytosol cannot be excluded, we tested the influence of a high cytosolic DIC (55 mmol $\cdot$ L^{-1}) on the carbonate chemistry inside the CV in a basic model version where C_i for calcite precipitation is supplied exclusively via CO_2

diffusion (model version Ib). The pH value of the cytosol and the initial value of the CV both are assumed to be seven as given by Anning *et al.* (1996) (cytosol: 6.9 ± 0.3; CV: 7.1 ± 0.3). The cytosolic salinity is presumed to be slightly lower than the one of seawater, because it is reduced by means of organic osmolytes (Bisson & Kirst, 1979; Kirst & Bisson, 1979). The salinity inside the CV is set to the value of seawater, because no data about compatible solutes inside the CV are available. Salinity and temperature remain constant throughout the model runs.
The carbonate system inside the CV is described via the following equations:

$$CO_2 + H_2O \underset{k_{-1}}{\overset{k_{+1}}{\rightleftharpoons}} H^+ + HCO_3^- \tag{S 1}$$

$$CO_2 + OH^- \underset{k_{-4}}{\overset{k_{+4}}{\rightleftharpoons}} HCO_3^- \tag{S 2}$$

$$CO_3^{2-} + H^+ \underset{k_{-5}^{H^+}}{\overset{k_{+5}^{H^+}}{\rightleftharpoons}} HCO_3^- \tag{S 3}$$

$$HCO_3^- + OH^- \underset{k_{-5}^{OH^-}}{\overset{k_{+5}^{OH^-}}{\rightleftharpoons}} CO_3^{2-} + H_2O \tag{S 4}$$

$$H_2O \underset{k_{-6}}{\overset{k_{+6}}{\rightleftharpoons}} H^+ + OH^- \tag{S 5}$$

The corresponding net reaction rates are denoted according to the numbers of the rate constants and describe the reactions (S 1) to (S 5) from right to left:

$$R_{1,CV} = -k_{+1}[CO_2]_{CV} + k_{-1}[H^+]_{CV}[HCO_3^-]_{CV} \tag{S 6}$$

$$R_{4,CV} = -k_{+4}[OH^-]_{CV}[CO_2]_{CV} + k_{-4}[HCO_3^-]_{CV} \tag{S 7}$$

$$R_{5,CV}^{H^+} = -k_{+5}^{H^+}[H^+]_{CV}[CO_3^{2-}]_{CV} + k_{-5}^{H^+}[HCO_3^-]_{CV} \tag{S 8}$$

$$R_{5,CV}^{OH^-} = -k_{+5}^{OH^-}[OH^-]_{CV}[HCO_3^-]_{CV} + k_{-5}^{OH^-}[CO_3^{2-}]_{CV}[H_2O]_{CV} \tag{S 9}$$

$$R_{6,CV} = -k_{+6} + k_{-6}[H^+]_{CV}[OH^-]_{CV} \tag{S 10}$$

Reaction rate constants are calculated via the equations given in Zeebe & Wolf-Gladrow (2001), values are listed in Table S2.
DIC and total alkalinity (TA) are defined as follows:

$$DIC = [CO_2]_{CV} + [HCO_3^-]_{CV} + [CO_3^{2-}]_{CV} \tag{S 11}$$

$$TA = [HCO_3^-] + 2\,[CO_3^{2-}]_{CV} + [OH^-]_{CV} - [H^+]_{CV} \tag{S 12}$$

The contribution of borate and several minor components to TA is neglected for the sake of simplicity. The concentrations of these compounds in cytosol and CV are not well known and do most probably differ from typical values in seawater.

(c) Active transport

The transport of molecules and ions across the CV membrane influences the corresponding concentrations inside the modelled CV. The rate by which these concentrations change is described by means of a Michaelis-Menten equation:

$$\mathrm{R}_{\mathrm{x}}^{\mathrm{T}} = \frac{1}{\mathrm{V_{CV}}} \frac{\mathrm{V_{max}[x]}}{\mathrm{K_M^x} + \mathrm{[x]}} \tag{S 13}$$

where $\mathrm{V_{CV}}$ stands for the volume of the CV, x for the transported substrate, $\mathrm{V_{max}}$ for the maximum transport rate, and $\mathrm{K_M^x}$ denotes the Michaelis-Menten constant, which describes the affinity of the transporter towards x.
When Ca^{2+} transport is concerned, $\mathrm{R}_{\mathrm{Ca^{2+}}}^{\mathrm{T}}$ is multiplied by the following cut-off function f($[Ca^{2+}]$).

$$\mathrm{f([Ca^{2+}])} = \frac{\tanh(1000 \, - \, 100\,[\mathrm{Ca^{2+}}])}{2} + \frac{1}{2} \tag{S 14}$$

where the $[Ca^{2+}]$ is given in mmol·L^{-1}. f($[Ca^{2+}]$) defines the maximum $[Ca^{2+}]$ ratio over the CV membrane to be 10^5, which was calculated by Langer *et al.* (2006) to be the maximum ratio that can be achieved by hydrolysis of ATP.
Each of the modelled transporters is dependent on the concentration of one transported substrate only (e. g. Ca^{2+} inside the cytosol), which can be done, when the cotransported or antitransported substrates (e. g. 2 H^+ inside the CV, in case of Ca^{2+} / 2 H^+ exchangers) are assumed to be abundant. Besides information on the maximum transport capacity as it is the case in the classical Michaelis-Menten equation, the parameter $\mathrm{V_{max}}$ contains further information on the kinetics of the cotransported, respectively antiported, substrate(s). During the first experiment part of model versions VI and VII, protons are transported via proton-pumping ATPases into the CV. We presumed, that neither ATP nor protons limit the transport and hence modelled proton import with a fixed rate here. A maximal proton concentration ratio of 10^5 across the membrane was assumed, constituting a very steep gradient, but allowing for a maximal effect of the Ca^{2+} import mechanism during the second model phase.
Our model does not integrate the membrane potential, because nothing is known about the ion composition around the CV membrane. Therefore, we decided to implement substrate transporters that exchange ions electrogenically neutral. Consequently, the stoichiometry assumed for Ca^{2+} / H^+ exchangers is 1 Ca^{2+} : 2 H^+ as it can for instance be found in the tonoplast of *Beta vulgaris* (Blumwald & Poole, 1986). This stoichiometry does not correspond to the one assumed for CAX-like Ca^{2+} / H^+ exchangers (1 : 3, Sze *et al.*, 2000) nor to that assumed for Ca^{2+}-ATPases (1 : 1-1.5, **?**Hauser & Barth, 2007). The latter transporter types do most probably exist in calcifying cells of *E. huxleyi* (see Section **??**). In case of SERCA-type Ca^{2+}-ATPases, stoichiometries of Ca^{2+} : H^+ vary with the underlying pH value (**?**Hauser & Barth, 2007). The latter transporter types do most probably exist in calcifying cells of *E. huxleyi* (see Section 2.1 of main document). In case of SERCA-type Ca^{2+}-ATPases, stoichiometries

of $Ca^{2+}:H^+$ vary with the underlying pH value (**?**Hauser & Barth, 2007). Proton-pumping ATPases could further influence bulk stoichiometries. We actually tested the influence of stoichiometries between 1 $Ca^{2+}:1$ H^+ and 1 $Ca^{2+}:3$ H^+ on a basic model version, where C_i is supplied passively via CO_2 diffusion and Ca^{2+} is imported actively via a Ca^{2+}/H^+ exchanger. While stoichiometries of 1 $Ca^{2+}:<2$ H^+ led to pH values that were too low for calcite precipitation, those of 1 $Ca^{2+}:>2$ H^+ led to very high pH values and very high $[CO_3^{2-}]$ inside the CV. A stoichiometry of 1 $Ca^{2+}:2$ H^+, in turn, led to reasonable results. Therefore, the latter stoichiometry which was assumed for some model versions is meaningful.

(d) Diffusion

CO_2 diffuses across the CV membrane in all model versions. Its diffusion rate $\mathrm{R}^{\mathrm{D}}_{\mathrm{CO_2}}$ is described as follows:

$$\mathrm{R}^{\mathrm{D}}_{\mathrm{CO_2}} = \gamma_{\mathrm{CO_2}} \frac{\mathrm{A_{CV}}}{\mathrm{V_{CV}}} \cdot ([\mathrm{CO_2}]_{\mathrm{CS}} - [\mathrm{CO_2}]_{\mathrm{CV}}) \qquad \text{(S 15)}$$

where $\gamma_{\mathrm{CO_2}}$ is the permeability coefficient of CO_2 given in Sültemeyer & Rinast (1996) for the plasma membrane of *Chlamydomonas reinhardtii* grown at ambient air and a pH of 7.8. $\mathrm{A_{CV}} / \mathrm{V_{CV}}$ reflects the surface to volume ratio of the CV, and $[CO_2]_{CS}$ and $[CO_2]_{CV}$ denote the $[CO_2]$ inside the cytosol (CS) and the CV, respectively.

(e) Calcite precipitation

The model considers the following reaction to describe calcite precipitation:

$$\mathrm{CO_3^{2-}} + \mathrm{Ca^{2+}} \rightarrow \mathrm{CaCO_3} \downarrow \qquad \text{(S 16)}$$

The corresponding precipitation rate is described via the following equations:

$$\mathrm{R_P} = \begin{cases} \mathrm{k_f}(\Omega - 1)^{\mathrm{n}} & \text{for } \Omega > 1 \\ 0 & \text{for } \Omega \leq 1 \end{cases} \qquad \text{(S 17)}$$

where the parameter n is given in Table 3 of Zuddas & Mucci (1994, 2.35), and $\mathrm{k_f}$ can be calculated from Figure 1 and Table 3 given in Zuddas & Mucci (1994) and the calculated CV morphology ($3.09 \cdot 10^{-5}$ mol·$\mathrm{L^{-1}}$·$\mathrm{s^{-1}}$).

(f) Model versions

The kinetic parameters used for all model runs are listed in Table S3.

Model version I: $Ca^{2+}/2\,H^{+}$ antiport. The activity of carbonic anhydrase (CA) in model version Ic was modelled via an acceleration factor of 10^4 for $\mathrm{R}_{1,\mathrm{CV}}$ (eq. (S 6)). This factor was taken from Thoms *et al.* (2001) who used it to model the CA inside the chloroplast.
The differential equations for model version I are constructed from the reaction rates given in equations (S 6) to (S 10), (S 13), (S 15), and (S 17):

$$\mathrm{d}[\mathrm{CO_2}]/\mathrm{dt}_{(\mathrm{I})} = \mathrm{R}_{1,\mathrm{CV}} + \mathrm{R}_{4,\mathrm{CV}} + \mathrm{R}^{\mathrm{D}}_{\mathrm{CO_2}} \tag{S 18}$$

$$\mathrm{d}[\mathrm{HCO_3^-}]/\mathrm{dt}_{(\mathrm{I})} = -\mathrm{R}_{1,\mathrm{CV}} - \mathrm{R}_{4,\mathrm{CV}} - \mathrm{R}^{\mathrm{H^+}}_{5,\mathrm{CV}} + \mathrm{R}^{\mathrm{OH^-}}_{5,\mathrm{CV}} \tag{S 19}$$

$$\mathrm{d}[\mathrm{CO_3^{2-}}]/\mathrm{dt}_{(\mathrm{I})} = \mathrm{R}^{\mathrm{H^+}}_{5,\mathrm{CV}} - \mathrm{R}^{\mathrm{OH^-}}_{5,\mathrm{CV}} - \mathrm{R}_{\mathrm{P}} \tag{S 20}$$

$$\mathrm{d}[\mathrm{H^+}]/\mathrm{dt}_{(\mathrm{I})} = -\mathrm{R}_{1,\mathrm{CV}} + \mathrm{R}^{\mathrm{H^+}}_{5,\mathrm{CV}} - \mathrm{R}_{6,\mathrm{CV}} \; - \; 2\,\mathrm{R}^{\mathrm{T}}_{\mathrm{Ca^{2+}}} \tag{S 21}$$

$$\mathrm{d}[\mathrm{OH^-}]/\mathrm{dt}_{(\mathrm{I})} = +\mathrm{R}_{4,\mathrm{CV}} + \mathrm{R}^{\mathrm{OH^-}}_{5,\mathrm{CV}} - \mathrm{R}_{6,\mathrm{CV}} \tag{S 22}$$

$$\mathrm{d}[\mathrm{Ca^{2+}}]/\mathrm{dt}_{(\mathrm{I})} = \mathrm{R}^{\mathrm{T}}_{\mathrm{Ca^{2+}}} \; - \; \mathrm{R}_{\mathrm{P}} \tag{S 23}$$

$$\mathrm{d}[\mathrm{PIC}]/\mathrm{dt}_{(\mathrm{I})} = \mathrm{R}_{\mathrm{P}} \tag{S 24}$$

For the following model versions, we will only give the equations that deviate from equations (S 18) to (S 24).

Model version II: $Ca^{2+}/2\,H^{+}$ antiport with active CO_2 import. The only differential equation that is changed compared to model version I, is the one describing the change of the $[CO_2]$:

$$\mathrm{d}[\mathrm{CO_2}]/\mathrm{dt}_{(\mathrm{II})} = \mathrm{R}_{1,\mathrm{CV}} + \mathrm{R}_{4,\mathrm{CV}} + \mathrm{R}^{\mathrm{D}}_{\mathrm{CO_2}} + \mathrm{R}^{\mathrm{T}}_{\mathrm{CO_2}} \tag{S 25}$$

Model version III: Import of Ca^{2+} and HCO_3^-. As mentioned in Section 3.1 of the main document, two different possibilities to import Ca^{2+} and HCO_3^- into the CV are concerned here. The only equation, in which the two model versions (IIIa and IIIb) differ from equations (S 18) to (S 24), is the one describing the change of $[\mathrm{HCO_3^-}]$.

$$\mathrm{d}[\mathrm{HCO_3^-}]/\mathrm{dt}_{(\mathrm{IIIa})} = -\mathrm{R}_{1,\mathrm{CV}} - \mathrm{R}_{4,\mathrm{CV}} - \mathrm{R}^{\mathrm{H^+}}_{5,\mathrm{CV}} + \mathrm{R}^{\mathrm{OH^-}}_{5,\mathrm{CV}} \; + \; \mathrm{R}^{\mathrm{T}}_{\mathrm{HCO_3^-}} \tag{S 26}$$

$$\mathrm{d}[\mathrm{HCO_3^-}]/\mathrm{dt}_{(\mathrm{IIIb})} = -\mathrm{R}_{1,\mathrm{CV}} - \mathrm{R}_{4,\mathrm{CV}} - \mathrm{R}^{\mathrm{H^+}}_{5,\mathrm{CV}} + \mathrm{R}^{\mathrm{OH^-}}_{5,\mathrm{CV}} \; + \; 2\,\mathrm{R}^{\mathrm{T}}_{\mathrm{Ca^{2+}}} \tag{S 27}$$

Since our model does not consider $[Na^+]$ and $[Cl^-]$, we neglect the export of these ion species.

Model version IV: Ca^{2+}/CO_3^{2-} symport. The modified differential equation for this model version reads:

$$\mathrm{d}[\mathrm{CO_3^{2-}}]/\mathrm{dt}_{(\mathrm{IV})} = \mathrm{R}^{\mathrm{H^+}}_{5,\mathrm{CV}} - \mathrm{R}^{\mathrm{OH^-}}_{5,\mathrm{CV}} + \mathrm{R}^{\mathrm{T}}_{\mathrm{Ca^{2+}}} - \mathrm{R}_{\mathrm{P}} \tag{S 28}$$

Model version V: Ca^{2+} and HCO_3^- import and H^+ export. Model version Va is based on a transport mechanism consisting of two decoupled transporters, namely a Ca^{2+} / 2 H^+ antiporter and a HCO_3^- / H^+ symporter. The modified differential equations read:

$$\mathrm{d[HCO_3^-]/dt_{(Va)}} = -\mathrm{R_{1,CV}} - \mathrm{R_{4,CV}} - \mathrm{R_{5,CV}^{H^+}} + \mathrm{R_{5,CV}^{OH^-}} + \mathrm{R_{HCO_3^-}^{T}} \quad \text{(S 29)}$$

$$\mathrm{d[H^+]/dt_{(Va)}} = -\mathrm{R_{1,CV}} + \mathrm{R_{5,CV}^{H^+}} - \mathrm{R_{6,CV}} + \mathrm{R_{HCO_3^-}^{T}} - 2\,\mathrm{R_{Ca^{2+}}^{T}} \quad \text{(S 30)}$$

Model version Vb mimics a theoretical transporter generating a transport of one Ca^{2+} and one HCO_3^- into the CV and one H^+ out of the CV. The differential equations are:

$$\mathrm{d[HCO_3^-]/dt_{(Vb)}} = -\mathrm{R_{1,CV}} - \mathrm{R_{4,CV}} - \mathrm{R_{5,CV}^{H^+}} + \mathrm{R_{5,CV}^{OH^-}} + \mathrm{R_{Ca^{2+}}^{T}} \quad \text{(S 31)}$$

$$\mathrm{d[H^+]/dt_{(Vb)}} = -\mathrm{R_{1,CV}} + \mathrm{R_{5,CV}^{H^+}} - \mathrm{R_{6,CV}} - \mathrm{R_{Ca^{2+}}^{T}} \quad \text{(S 32)}$$

Model version VI: Ca^{2+} / H^+ exchange after import of H^+. For the first part of this model version, by means of which the proton gradient across the CV membrane is established, the following equations are used:

$$\mathrm{d[H^+]/dt_{(VI)}} = -\mathrm{R_{1,CV}} + \mathrm{R_{5,CV}^{H^+}} - \mathrm{R_{6,CV}} + \mathrm{R_{H^+}^{T}} \quad \text{(S 33)}$$

$$\mathrm{d[Ca^{2+}]/dt_{(VI)}} = -\mathrm{R_P} \quad \text{(S 34)}$$

$$\mathrm{d[PIC]/dt_{(VI)}} = \mathrm{R_P} \quad \text{(S 35)}$$

The second model part, during which the established proton gradient is used to import Ca^{2+}, the equations given for model version I are considered.

Model version VII: Ca^{2+} and HCO_3^- import and H^+ export after import of H^+. The acidification part of this model is described via the equations given for model version VI (eqs. S 33 - S 35). For the second part in turn, the equations of model version Vb (eqs. (S 31) - (S 32)) are used.

Appendix to Results and Discussion

Figures S2 to S6 give the model outputs to all model versions, except for model version Ic which was shown already in the main document.
At Time = 0 s, the preset initial conditions are given. During the presented time regime, the modelled DIC, TA, pH, C_i, Ω, and Ca^{2+} approach the steady state values listed in Table 4 of the main manuscript.

References

Anning, T., Nimer, M., Merrett, M. J., & Brownlee, C. 1996. Costs and benefits of calcification in coccolithophorids. *J. Marine Syst.*, **9**, 45–56.

Bisson, M. A., & Kirst, G. O. 1979. Osmotic adaption in the marine alga *Griffithsia monilis* (Rhodophyceae): The role of ions and organic compounds. *Aust. J. Plant Physiol.*, **6**, 523–538.

Blumwald, E., & Poole, R. J. 1986. Kinetics of Ca^{2+} / H^{+} antiport in isolated tonoplast vesicles from storage tissue of *Beta vulgaris* L. *Plant Physiol.*, **80**(Feb.), 727–731.

Brownlee, C., Davies, M., Nimer, N., Dong, L. F., & Merrett, M. J. 1995. Calcification, photosynthesis and intracellular regulation in *Emiliania huxleyi*. *Bulletin de l'Institut oceanographique*, **14**, 19–35.

Dixon, G. K., Brownlee, C., & Merrett, M. J. 1989. Measurement of internal pH in the coccolithophore *Emiliania huxleyi* using 2', 7'-bis-(2-carboxyethyl)-5 (and-6) carboxyfluorescein acetoxymethylester and digital imaging microscopy. *Planta*, **178**, 443–449.

Gussone, N., Langer, G., Thoms, S., Nehrke, G., Eisenhauer, A., Riebesell, U., & Wefer, G. 2006. Cellular calcium pathways and isotope fractionation in *Emiliania huxleyi*. *Geology*, **34**, 625.

Hauser, K, & Barth, A. 2007. Side-chain protonation and mobility in the sarcoplasmic reticulum Ca^{2+}-ATPase: Implications for proton countertransport and Ca^{2+} release. *Biophys. J.*, **93**(Nov.), 3259–3270.

Kirst, G. O., & Bisson, M. A. 1979. Regulation of turgor pressure in marine algae: ions and low-molecular-weight organic compounds. *Aust. J. Plant Physiol.*, **6**, 539–556.

Langer, G., Gussone, N., Nehrke, G., Riebesell, U., Eisenhauer, A., Kuhnert, H., Rost, B., Trimborn, S., & Thoms, S. 2006. Coccolith strontium to calcium ratios in *Emiliania huxleyi*: The dependence on seawater strontium and calcium concentrations. *Limnol. Oceanogr.*, **51**(1), 310–320.

Sekino, K., & Shiraiwa, Y. 1994. Accumulation and utilization of dissolved inorganic carbon by a marine unicellular coccolithophorid, *Emiliania huxleyi*. *Plant Cell Physiol.*, **35**(3), 353–361.

Sültemeyer, D., & Rinast, K.-A. 1996. The CO_2 permeability of the plasma membrane of *Chlamydomonas reinhardtii*: mass-spectrometric ^{18}O-exchange measurements from $^{13}C^{18}0_2$ in suspensions of carbonic anhydrase-loaded plasma-membrane vesicles. *Planta*, **200**, 358–368.

Sze, H., Liang, F., Hwang, I., Curran, A. C., & Harper, J. F. 2000. Diversity and regulation of plant Ca^{2+} pumps: insights from expression in yeast. *Annu. Rev. Plant Biol.*, **51**, 433–462.

Thoms, S., Pahlow, M., & Wolf-Gladrow, D. A. 2001. Model of the carbon concentrating mechanism in chloroplasts of eukaryotic algae. *J. theor. Biol.*, **208**, 295–313.

van der Wal, P., de Jong, E W, Westbroek, P., de Bruijn, W. C., & Mulder-Stapel, A. A. 1983a. Ultrastructural polysaccharide localization in calcifying and naked cells of the coccolithophorid *Emiliania huxleyi*. *Protoplasma*, **118**, 157–168.

Young, J. R. 2009. *Coccoliths on Emiliania huxleyi homepage*. `www.noc.soton.ac.uk/soes/staff/tt/eh/coccoliths.html`. accessed 25.11.2011.

Young, J. R., & Ziveri, P. 2000. Calculation of coccolith volume and its use in calibration of carbonate flux estimates. *Deep-Sea Res. Pt. II*, **47**(9-11), 1679–1700.

Zeebe, R. E., & Wolf-Gladrow, D. A. 2001. *CO_2 in seawater: equilibrium, kinetics, isotopes*. Amsterdam: Elsevier Science Ltd.

Zuddas, P., & Mucci, A. 1994. Kinetics of calcite precipitation from seawater: I. A classical chemical kinetics description for strong electrolyte solutions. *Geochim. Cosmochim. Ac.*, **58**(20), 4353–4362.

Table S 1: *Values for [Ca^{2+}], DIC, pH, salinity (S), and temperature (θ) inside the cytosol (CS) and the CV. The concentrations of carbonate species are calculated from DIC and pH (equilibrium values). Values put in parantheses are those for model version Ib, which is based on 55 mmol·L^{-1} DIC in CS.*

Parameter	Value CS	Value CV
[Ca^{2+}] (mmol·L^{-1})	$100 \cdot 10^{-6}$ (Brownlee *et al.*, 1995)	0.5 (Gussone *et al.*, 2006)
DIC (mmol·L^{-1})	2 (55 in Ib)	2
pH	7 (Dixon *et al.*, 1989)	7 (Anning *et al.*, 1996)
S	30	35
θ (°C)	15	15
CO_2 (μmol·L^{-1})	169 (4 656 in Ib)	163
HCO_3^- (μmol·L^{-1})	1 820 (50 000 in Ib)	1 823
CO_3^{2-} (μmol·L^{-1})	12.9 (355 in Ib)	14.5

Table S 2: *Reaction rate constants of the carbonate system. Since the salinity of the cytosol (CS) and the CV are assumed to differ (CS: 30, CV: 35), the rate constants are listed separately.*

Rate constant	Value CS	Value CV
k_{+1} (s^{-1})	$14.2 \cdot 10^{-3}$	
k_{-1} ($L \cdot mol^{-1} \cdot s^{-1}$)	$12.9 \cdot 10^{3}$	$12.4 \cdot 10^{3}$
k_{+4} ($L \cdot mol^{-1} \cdot s^{-1}$)	$2.86 \cdot 10^{3}$	$2.89 \cdot 10^{3}$
k_{-4} (s^{-1})	$5.96 \cdot 10^{-5}$	$6.23 \cdot 10^{-5}$
$k_{+5}^{H^+}$ ($L \cdot mol^{-1} \cdot s^{-1}$)	$4.89 \cdot 10^{10}$	$4.87 \cdot 10^{10}$
$k_{-5}^{H^+}$ (s^{-1})	35.5	39.9
$k_{+5}^{OH^-}$ ($L \cdot mol^{-1} \cdot s^{-1}$)	$5.87 \cdot 10^{9}$	$5.85 \cdot 10^{9}$
$k_{-5}^{OH^-}$ (s^{-1})	$1.85 \cdot 10^{5}$	$1.79 \cdot 10^{5}$
k_{+6} ($mol \cdot L^{-1} \cdot s^{-1}$)	$1.43 \cdot 10^{-3}$	$1.44 \cdot 10^{-3}$
k_{-6} ($L \cdot mol^{-1} \cdot s^{-1}$)	$6.27 \cdot 10^{10}$	$5.73 \cdot 10^{10}$

Table S 3: *Kinetic parameter values for all model versions.*

Parameter	Value	Version
γ_{CO_2} (m·s^{-1})	$1.8{\cdot}10^{-5}$ (Sültemeyer & Rinast, 1996)	all
$V_{max(Ca^{2+}/2H^+)}$(mol·s^{-1})	$0.54{\cdot}10^{-15}$	(Ia)
$K_m^{Ca^{2+}}{}_{(Ca^{2+}/2H^+)}$(mol·L^{-1})	$42{\cdot}10^{-6}$ (Blumwald & Poole, 1986)	
$V_{max(Ca^{2+}/2H^+)}$(mol·s^{-1})	$2.6{\cdot}10^{-15}$	(Ib, Ic)
$K_m^{Ca^{2+}}{}_{(Ca^{2+}/2H^+)}$(mol·L^{-1})	$42{\cdot}10^{-6}$ (Blumwald & Poole, 1986)	
$V_{max(Ca^{2+}/2H^+)}$(mol·s^{-1})	$2.6{\cdot}10^{-15}$	(II)
$K_m^{Ca^{2+}}{}_{(Ca^{2+}/2H^+)}$(mol·L^{-1})	$42{\cdot}10^{-6}$ (Blumwald & Poole, 1986)	
$V_{max(CO_2)}$(mol·s^{-1})	$1.4{\cdot}10^{-15}$	
$K_m^{CO_2}{}_{(CO_2)}$(mol·L^{-1})	$0.1{\cdot}10^{-6}$	
$V_{max(Ca^{2+}/2Na^+)}$(mol·s^{-1})	$2.6{\cdot}10^{-15}$	(IIIa)
$K_m^{Ca^{2+}}{}_{(Ca^{2+}/2Na^+)}$(mol·L^{-1})	$42{\cdot}10^{-6}$	
$V_{max(HCO_3^-/Cl^-)}$(mol·s^{-1})	$13{\cdot}10^{-18}$	
$K_m^{HCO_3^-}{}_{(HCO_3^-/Cl^-)}$(mol·L^{-1})	$0.1{\cdot}10^{-3}$	
$V_{max(Ca^{2+}/2HCO_3^-)}$(mol·s^{-1})	$2.6{\cdot}10^{-15}$	(IIIb)
$K_m^{Ca^{2+}}{}_{(Ca^{2+}/2H^+)}$(mol·L^{-1})	$42{\cdot}10^{-6}$ (Blumwald & Poole, 1986)	
$V_{max(Ca^{2+}/CO_3^{2-})}$(mol·s^{-1})	$2.6{\cdot}10^{-15}$	(IV)
$K_m^{Ca^{2+}}{}_{(Ca^{2+}/CO_3^{2-})}$(mol·L^{-1})	$42{\cdot}10^{-6}$	
$V_{max(Ca^{2+}/2H^+)}$(mol·s^{-1})	$2.6{\cdot}10^{-15}$	(Va)
$K_m^{Ca^{2+}}{}_{(Ca^{2+}/2H^+)}$(mol·L^{-1})	$42{\cdot}10^{-6}$ (Blumwald & Poole, 1986)	
$V_{max(HCO_3^-/H^+)}$(mol·s^{-1})	$6.52{\cdot}10^{-18}$	
$K_m^{HCO_3^-}{}_{(HCO_3^-/H^+)}$(mol·L^{-1})	$0.1{\cdot}10^{-3}$	
$V_{max(Ca^{2+}/HCO_3^-/H^+)}$(mol·s^{-1})	$2.6{\cdot}10^{-15}$	(Vb)
$K_m^{Ca^{2+}}{}_{(Ca^{2+}/HCO_3^-/H^+)}$(mol·L^{-1})	$42{\cdot}10^{-6}$	
$V_{(H^+)}$(mol·L^{-1}·s^{-1})	$0.02{\cdot}10^{-3}$	(VI)
$V_{max(Ca^{2+}/2H^+)}$(mol·s^{-1})	$1.0{\cdot}10^{-15}$	
$K_m^{Ca^{2+}}{}_{(Ca^{2+}/2H^+)}$(mol·L^{-1})	$42{\cdot}10^{-6}$ (Blumwald & Poole, 1986)	
$V_{(H^+)}$(mol·L^{-1}·s^{-1})	$0.02{\cdot}10^{-3}$	(VII)
$V_{max(Ca^{2+}/HCO_3^-/H^+)}$(mol·s^{-1})	$3.2{\cdot}10^{-15}$	
$K_m^{Ca^{2+}}{}_{(Ca^{2+}/HCO_3^-/H^+)}$(mol·L^{-1})	$42{\cdot}10^{-6}$ (Blumwald & Poole, 1986)	

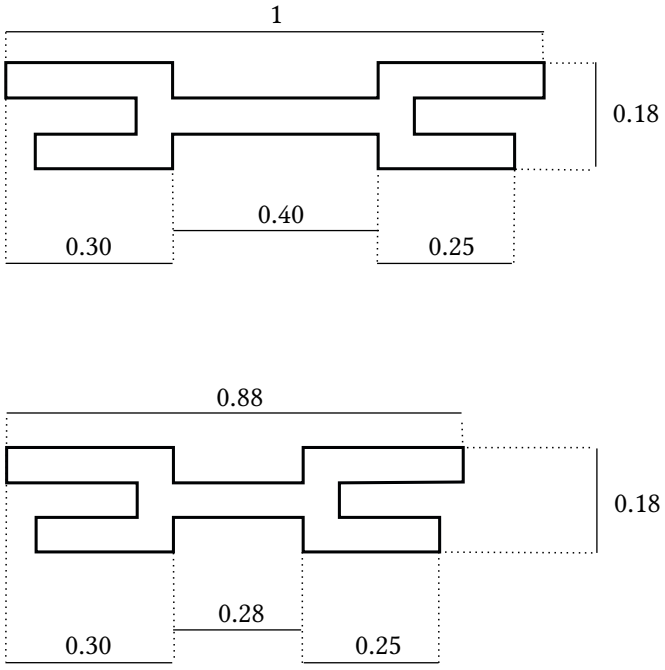

Figure S 1: *Simplified shape of the CV. The large diameter size of the coccolith is scaled to 1.*

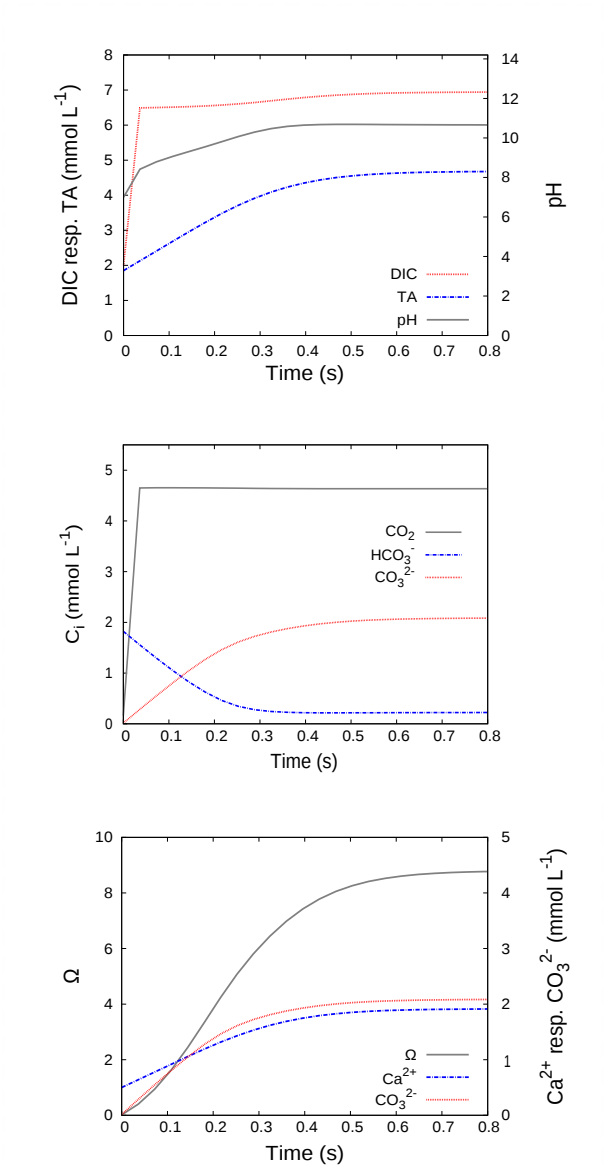

Figure S 2: *Model outputs to model version Ib and II. DIC in the cytosol was increased to 55 mmol* L^{-1} *in Ib. Model version II is based on an active* CO_2 *import into the CV. Development of DIC, TA,* Ω*,* Ca^{2+} *and the individual DIC species' concentrations inside the CV during the first 0.8 second of the model run.*

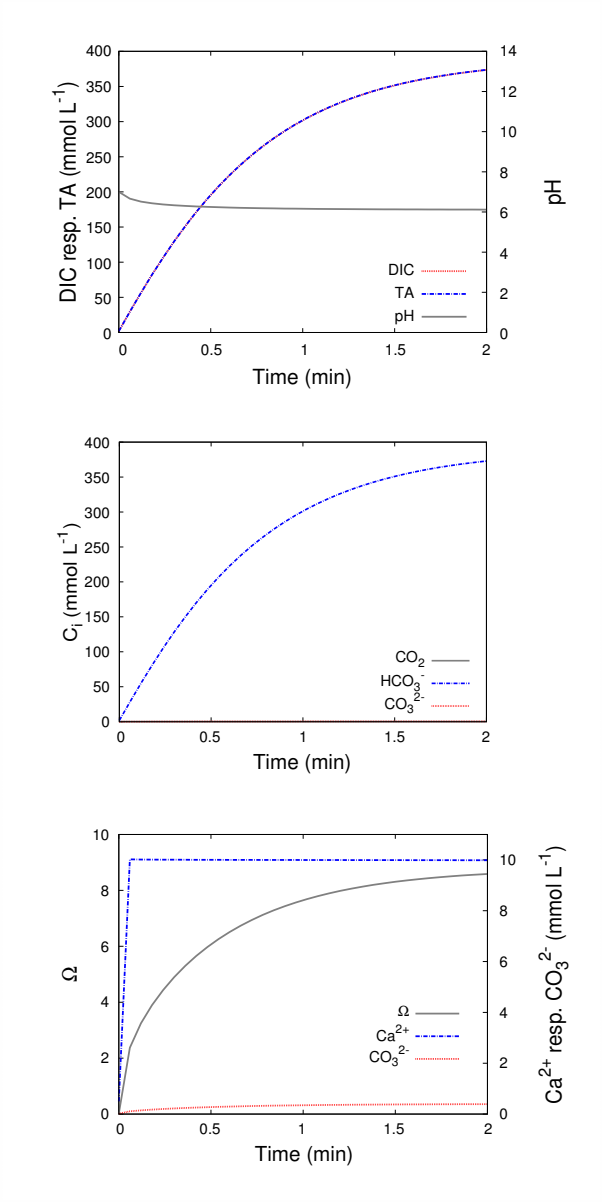

Figure S 3: *Model outputs to model version IIIa.* Ca^{2+} *and* HCO_3^- *cross the CV membrane independently of each other, while no* H^+ *are exported from the CV.*

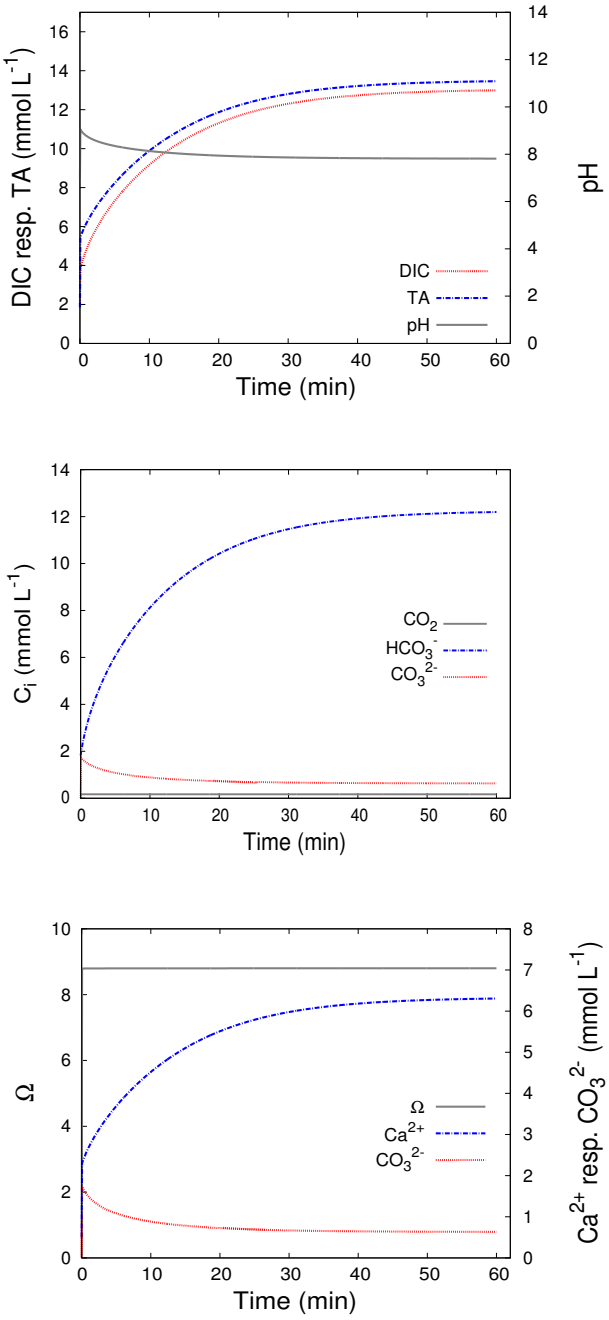

Figure S 4: *Model outputs to version IV, Va, and Vb.* Ca^{2+} *and* CO_3^{2-} *are actively imported in version IV. Version V assumes an import of* Ca^{2+}, HCO_3^-, *and an export of* H^+, *once via two transporters (V a) and once by means of one complex transporter (V b).*

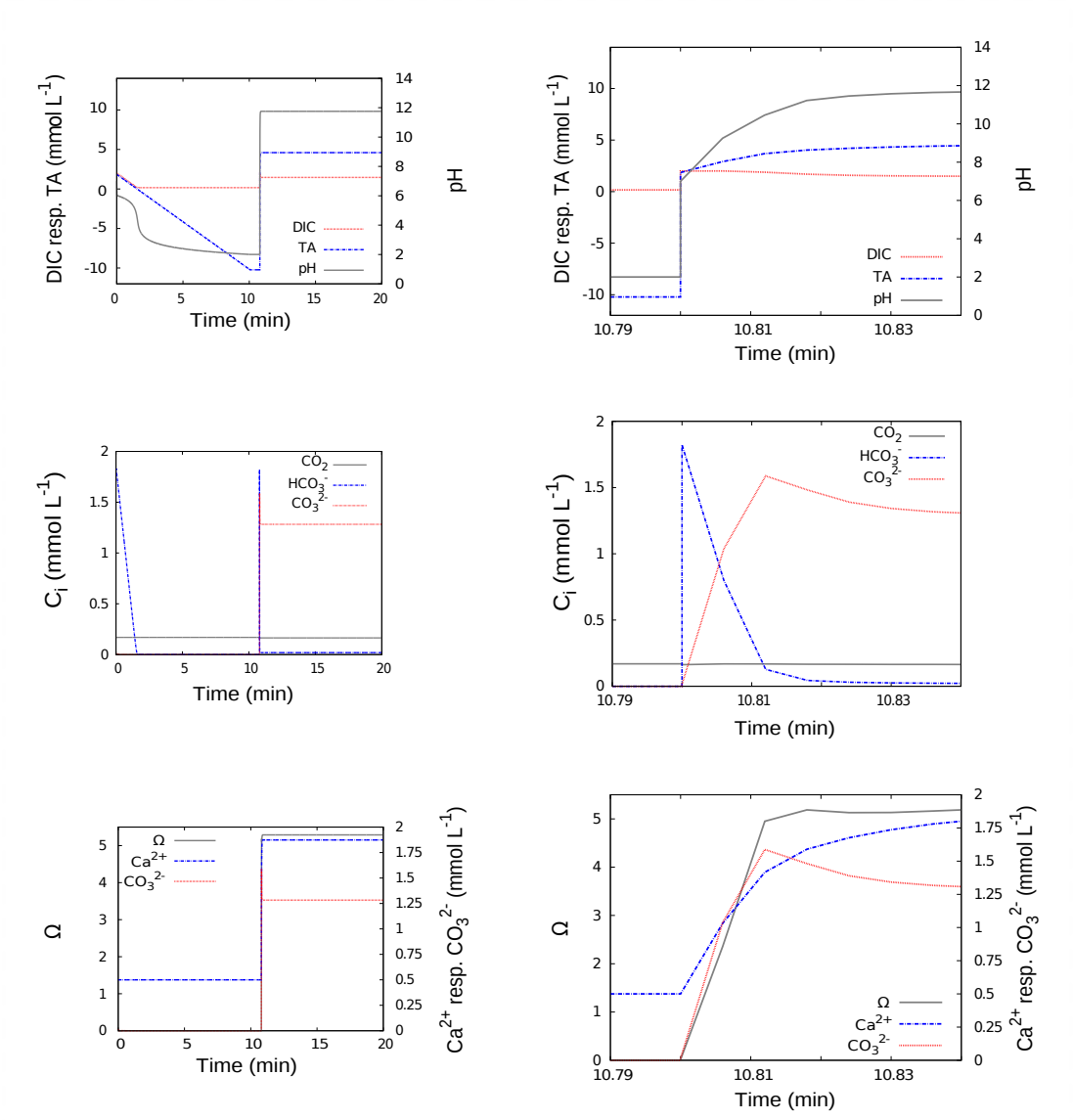

Figure S 5: *Results to model version VI. The plots on the left hand side present the first 20 minutes of the model run, while on the right hand side, the time slot, during which the ATPase activity is stopped and the Ca^{2+} / 2 H^{+} exchanger starts its activity, is shown explicitly. CO_2 diffuses across the membrane in both stages.*

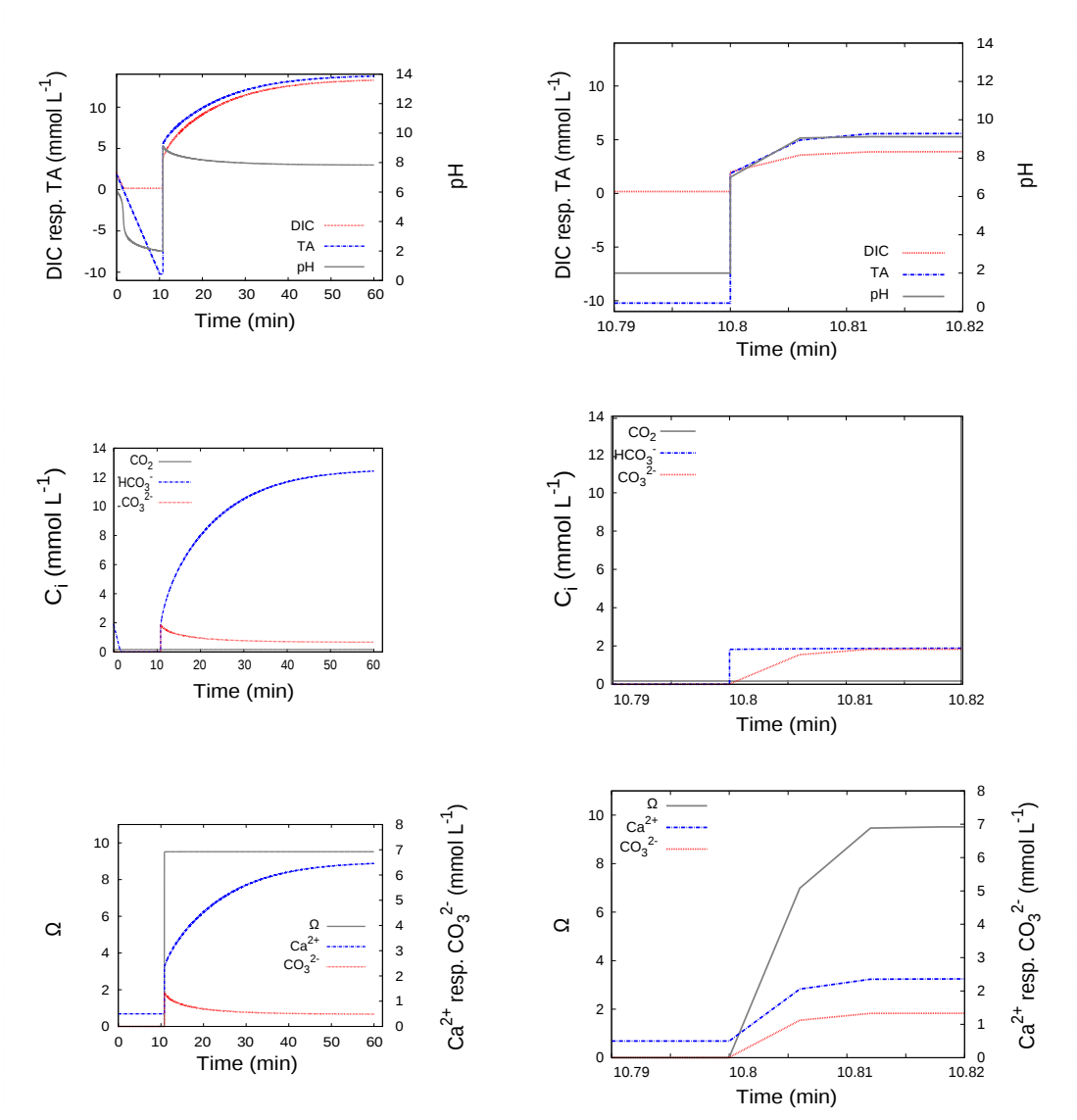

Figure S 6: *Results to model version VII. Ca^{2+}, HCO_3^- and H^+ actively cross the CV membrane, after the establishment of a proton gradient across the CV membrane by means of an ATPase. CO_2 diffuses across the membrane in both stages. The plots on the left hand side present the whole model run, while on the right hand side, the time slot, during which the ATPase activity is stopped and the Ca^{2+} / HCO_3^- / H^+ exchanger starts its activity, is shown in more detail.*